

A Novel Joint Angle-Range-Velocity Estimation Method for MIMO-OFDM ISAC Systems

Zichao Xiao, Rang Liu, *Graduate Student Member, IEEE*, Ming Li, *Senior Member, IEEE*,
and Qian Liu, *Member, IEEE*

Abstract—Integrated sensing and communications (ISAC) is emerging as a key technique for next-generation wireless systems. In order to enable ubiquitous mobile network and widely deployed base stations with radar sensing functionality, using standard multiple-input multiple-output (MIMO) orthogonal frequency division multiplexing (OFDM) transmitter architectures and waveforms to achieve both satisfactory sensing and communication performance is a crucial task for practical implementations of ISAC. In this paper, we propose a novel joint angle-range-velocity estimation algorithm for the considered MIMO-OFDM ISAC system. The approach is based on classical MIMO-OFDM waveforms widely adopted in wireless communications. Specifically, the angle-range-velocity information of potential targets is jointly extracted by utilizing all the received echo signals in a coherent processing interval (CPI). Therefore, the proposed joint estimation algorithm can achieve larger processing gains and higher resolution by fully exploiting echo signals and jointly estimating the angle-range-velocity information. Theoretical analysis for maximum unambiguous range, resolution, and processing gains are provided to verify the advantages of the proposed joint estimation algorithm. Finally, extensive numerical experiments are presented to demonstrate that the proposed estimation approach can achieve significantly lower root-mean-square-error (RMSE) of angle/range/velocity estimation for both single-target and multi-target scenarios.

Index Terms—Integrated sensing and communications (ISAC), multiple-input multiple-output orthogonal frequency division multiplexing (MIMO-OFDM), parameter estimation.

I. INTRODUCTION

Next-generation wireless systems are expected to develop beyond traditional communication service providers and further facilitate a series of innovative applications, such as intelligent transportation, manufacturing, and healthcare, etc. These emerging applications not only impose higher demands on communication performance but also require more robust sensing capabilities. In addition, with the exponential growth of wireless devices and communication demands, spectral resources are becoming increasingly scarce. The radar frequency bands, which have large portions of available spectrum, is therefore regarded as one promising choice for communication use. From a technical point of view, the technology trend of wireless communication and radar sensing also shows a high degree of consistency: The pursuit of higher frequencies, wider

bandwidths, larger antenna arrays, more attention to line-of-sight channels, and distributed dense deployment. Therefore, wireless communication and radar sensing exhibit more and more commonality and similarity in system design, hardware platform, signal processing, etc., which lays a solid technical foundation for the integration of these two functionalities. Integrated sensing and communications (ISAC), which focuses on the coexistence, cooperation, and co-design of these two systems, has recently emerged as one of key enabling technologies for the sixth generation (6G) wireless systems [1], [2] and has aroused extensive research attentions from both academia and industry [3]–[6].

To achieve satisfactory communication and sensing performance, the dual-functional transmit waveform and associated echo signal processing approaches are very crucial in ISAC systems. Existing research is generally based on traditional radar systems, communication systems, or dual-functional systems that require special customization. In specific, radar-based ISAC systems focus on embedding communication symbols into existing radar sensing signals, e.g., linear frequency modulated continuous wave (LFMCW) [7], [8] and frequency-hopping (FH) radar [9], [10]. Communication-based ISAC systems rely on existing hardware architectures and signal structures for communications to perform dual-functional tasks, e.g., the investigations based on 802.11ad standard waveforms [11], [12] and the studies for perceptive mobile networks (PMNs) [13], [14]. In addition, the dual-functional systems not restricted to existing radar/communication infrastructures have also been investigated [15]–[17]. Owing to the ubiquitous wireless communication networks, communication-based designs will greatly facilitate practical development of ISAC. Therefore, the use of communication transmission architectures and waveforms to implement ISAC is very promising to efficiently and cost-effectively empower wireless networks with sensing capabilities.

In existing commercial wireless communication networks, orthogonal frequency division multiplexing (OFDM) has been widely adopted as the dominant waveform [18]. Benefiting from its capabilities to overcome frequency selective fading and support high spectral efficiency, OFDM waveforms provide much higher information transmission rate for wireless communications. On the other hand, OFDM waveforms can support satisfactory radar sensing performance, e.g., by harnessing frequency diversity, OFDM waveforms can enhance target detection [19] or parameter estimation [20]; by utilizing the cyclic prefixed (CP) structure, OFDM waveforms can entirely eliminate the inter-range-cell interference for range

Z. Xiao, R. Liu, and M. Li are with the School of Information and Communication Engineering, Dalian University of Technology, Dalian 116024, China (e-mail: xiaozichao@mail.dlut.edu.cn; liurang@mail.dlut.edu.cn; mli@dlut.edu.cn).

Q. Liu is with the School of Computer Science and Technology, Dalian University of Technology, Dalian 116024, China (e-mail: qianliu@dlut.edu.cn).

reconstruction [21]-[23]. Therefore, the OFDM waveform has been recognized as an attractive candidate for realizing ISAC in practice. Considering that OFDM waveforms are communication-oriented, how to realize high-performance radar sensing functionality based on existing OFDM communication networks is a key task to facilitate practical applications.

Many researchers have explored OFDM waveform design and echo signal processing algorithms for ISAC systems, in which the dual-functional OFDM waveform is optimized to simultaneously perform single/multiple-user communications and target detection/estimation/tracking. In specific, to realize target parameter estimation using OFDM communication signals, the seminal work [24] presented a novel echo signal processing algorithm for estimating the range and velocity of potential targets. Then, super-resolution methods were presented in [25]-[27], and a deep-learning based method for terahertz systems was developed in [28]. In addition, the power allocation problem was investigated [29]-[31] in order to achieve a better performance trade-off for OFDM ISAC systems. While above works [24]-[31] verified the feasibility of using OFDM waveforms to realize ISAC, they only focused on the scenario of a single-antenna transmitter.

Multi-input multi-output (MIMO) architecture has been widely employed in both communication and radar sensing systems, and is therefore regarded as one key feature of future ISAC systems. The MIMO architecture provides additional spatial degrees-of-freedom (DoFs), which can be exploited to achieve spatial multiplexing, spatial diversity, and beamforming gain for both communication and radar sensing [32], [33]. However, unlike the waveforms used in traditional MIMO radar systems, the dual-functional waveforms in ISAC systems should carry communication symbols, whose randomness will inevitably destroy the orthogonality between signals emitted from different antennas. In the sequel, transmitted dual-functional signals will be mixed together in the spatial domain, which causes great difficulties in radar target parameter estimation. Therefore, sophisticated echo signal processing algorithms are required to estimate the potential target parameters based on MIMO-OFDM waveforms in ISAC systems.

In order to maintain orthogonality between signals emitted from different antennas, the authors in [34] proposed to allocate different subcarriers to each antenna, i.e., the subcarriers are non-overlapping among the antennas, which allows to employ echo signal processing algorithms developed for MIMO radar systems. However, since frequency resources are not fully exploited, it is obvious that the communication capacity will be significantly reduced. To overcome this problem, recent work [35] proposed a novel echo signal processing approach to extract target parameters contained in the mixed and overlapping MIMO-OFDM signals. Although this approach fully utilizes spatial and frequency resources in MIMO-OFDM waveforms, the estimation of angle and range only exploits the received echo signals during one OFDM symbol. Compared with traditional radar sensing algorithm that is usually performed during one coherent processing interval (CPI) with multiple OFDM symbols, this approach [35] will suffer from

lower signal processing gains since it does not fully exploit resources in the temporal domain. Moreover, the angle-range-velocity of potential targets is successively estimated in [35], which will inevitably lead to error propagation on parameter estimation. Therefore, echo signal processing and parameter estimation algorithm should be further investigated to improve the estimation performance for MIMO-OFDM ISAC systems.

Motivated by the above findings, in this paper we focus on the echo signal processing for better parameter estimation performance in MIMO-OFDM ISAC systems. In particular, we consider a typical MIMO-OFDM ISAC system, in which a multi-antenna base station (BS) transmits OFDM waveforms to simultaneously serve multiple single-antenna communication users and estimate the parameters of multiple point-like targets via processing received echo signals. Our goal is to propose a joint angle-range-velocity estimation approach to fully exploit available information in spatial, frequency, and temporal domains of the MIMO-OFDM echo signals. The main contributions of this paper are presented as follows.

- First, we establish the models for the transmitted signals, the received communication signals at communication users, and the received echo signals at the BS for the considered MIMO-OFDM ISAC system. Based on the signal models, we develop a novel echo signal processing method to estimate the parameters of potential targets. In specific, the angle-range-velocity is jointly estimated by utilizing all the received echo signals during one CPI, which can bring substantial processing gains compared with the existing approach that only uses one OFDM symbol. Moreover, through joint estimation from three dimensions instead of successively determining its parameters, the sensing resolution can be significantly improved.
- Next, we provide theoretical analysis for the maximum unambiguous range, resolution, and processing gain achieved by the proposed joint estimation approach, from which we gain valuable insights about the achievable sensing performance improvements.
- Finally, simulation results are presented to validate the feasibility and advantages of the proposed joint estimation method. Compared to existing work, the proposed method provides superior performance for angle-range-velocity estimation in terms of root-mean-squared-error (RMSE) and signal-to-noise ratio (SNR) gains.

The rest of this paper is organized as follows. Section II introduces the system model, the transmitted signal model and the received signal models for communications and sensing, respectively. The proposed joint angle-range-velocity estimation method is described in Sec. III, and associated theoretical performance analysis is presented in Sec. IV. Simulation results are shown in Sec. V, and finally conclusions are provided in Section VI.

Notation: Lower-case, boldface lower-case, and upper-case letters indicate scalars, column vectors, and matrices, respectively. $(\cdot)^T$ and $(\cdot)^H$ denote the transpose and transpose-conjugate operations, respectively. $\mathbb{E}\{\cdot\}$ represents statistical expectation. $|a|$ is the magnitude of a scalar a . \mathbb{Z} and \mathbb{C} denote

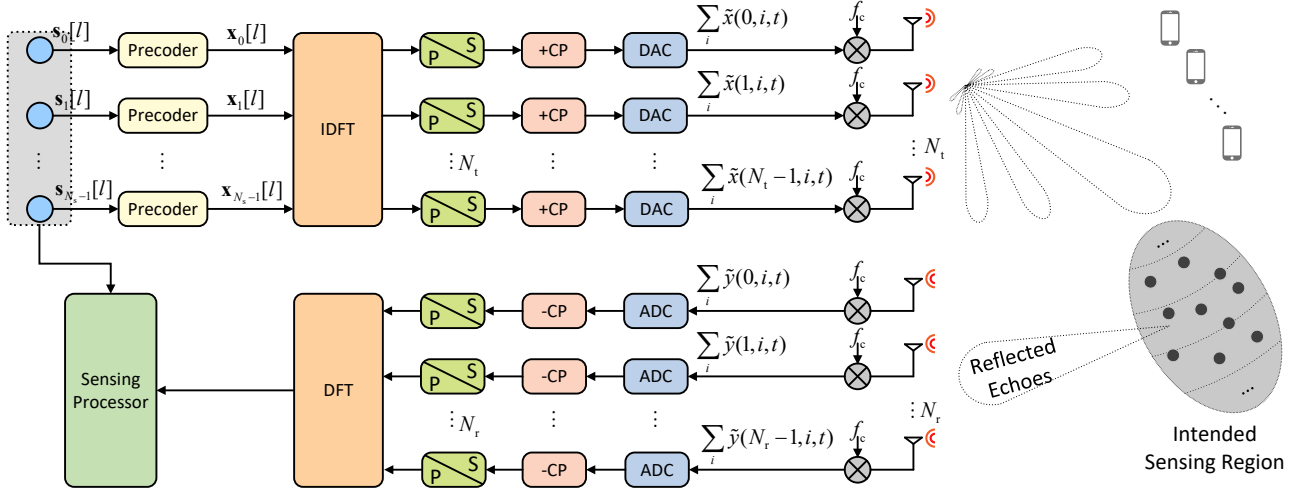


Fig. 1: The considered MIMO-OFDM ISAC system.

the set of integers and complex numbers, respectively. \sqrt{a} returns the square root of scalar a . $\lfloor \cdot \rfloor$ rounds a real number to the nearest integer less than or equal to it.

II. SYSTEM MODEL

We consider a mono-static MIMO-OFDM ISAC system as illustrated in Fig. 1, in which a dual-functional BS equipped with two separate uniform linear arrays (ULAs) of N_t transmit antennas and N_r receive antennas simultaneously performs downlink multi-user communications and target parameter estimation. We assume that the BS operates in a full-duplex mode with perfect self-interference (SI) cancellation given advanced full-duplex techniques [36]-[38]. Specifically, the BS transmits OFDM waveforms to communicate with K single-antenna users and sense multiple point-like targets, and meanwhile processes the received echo signals for estimating the angle-range-velocity information of potential targets.

A. Transmitted Signal Model

In the considered OFDM system, the central carrier frequency is f_c and the wavelength is $\lambda_c = c/f_c$, where c denotes the speed of light. There are N_s -subcarriers with frequency spacing $\Delta f = 1/T_d$, where T_d is the OFDM symbol duration. We denote the communication symbol vector of the i -th subcarrier at the l -th symbol-slot as $\mathbf{s}_i[l] \in \mathbb{C}^K$, $i = 0, \dots, N_s - 1$, $l = 0, \dots, L - 1$, where L is the frame length of one CPI. Each element of $\mathbf{s}_i[l]$ is independently selected from quadrature amplitude modulation (QAM) constellation, $\mathbb{E}\{\mathbf{s}_i[l]\} = \mathbf{0}$ and $\mathbb{E}\{\mathbf{s}_i[l]\mathbf{s}_i^H[l]\} = \mathbf{I}_K$. The transmitted symbols are firstly precoded through precoders $\mathbf{W}_i \triangleq [\mathbf{w}_{i,1}, \dots, \mathbf{w}_{i,K}] \in \mathbb{C}^{N_t \times K}$, $\forall i$, in order to focus the beams towards the communication users and potential targets. Thus, the transmitted signal on the i -th subcarrier during the l -th OFDM symbol can be expressed as

$$\mathbf{x}_i[l] \triangleq \begin{bmatrix} x(0, i, l) \\ x(1, i, l) \\ \vdots \\ x(N_t - 1, i, l) \end{bmatrix} = \mathbf{W}_i \mathbf{s}_i[l], \quad (1)$$

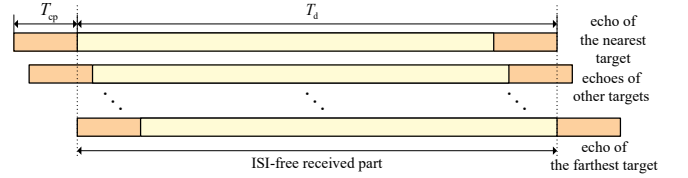


Fig. 2: The received echoes of one CP-based OFDM symbol.

where $x(n, i, l)$ denotes the signal transmitted by the n -th antenna, $n = 0, \dots, N_t - 1$.

As described in Fig. 1, the baseband signals (1) in the frequency domain are transformed into the temporal domain by N_s -point inverse discrete Fourier transform (IDFT). Then, a cyclic prefix (CP) of N_{cp} points and T_{cp} duration is inserted in order to avoid inter-symbol interference (ISI) for both communication and sensing. We know that the CP length should be greater than the channel impulse response length to avoid ISI for downlink communications. Meanwhile, in order to eliminate ISI at the sensing receiver, the CP duration should also be larger than the roundtrip delay between the nearest target and the furthest target, which can be easily obtained as illustrated in Fig. 2. Then, after being processed by digital-to-analog converters (DACs), the baseband analog signal transmitted by the n -th antenna on the i -th subcarrier is expressed as

$$\tilde{x}(n, i, t) \triangleq \sum_{l=0}^{L-1} x(n, i, l) e^{j2\pi i \Delta f t} \text{rect}\left(\frac{t - lT}{T}\right), \quad (2)$$

where $T \triangleq T_d + T_{cp}$ is the total symbol duration and $\text{rect}(t/T)$ denotes a rectangular pulse of duration T . Finally, the baseband analog signal is up-converted to the radio frequency (RF) domain via N_t RF chains with carrier frequency f_c and then emitted through the antennas.

B. Communication Signal Model

After propagating through downlink communication channels, the OFDM signals are received by the single-antenna

users and then demodulated into communication symbols. In particular, the communication receiver employs a series of operations including down-converting, analog-to-digital converting (ADC), removing the CP, and N_s -point DFT to process the received communication signals. For the k -th user, the frequency-domain signal on the i -th subcarrier during the l -th OFDM symbol can be written as

$$y_{i,k}[l] \triangleq \mathbf{h}_{i,k}^H \mathbf{W}_i \mathbf{s}_i[l] + z_{i,k}[l], \quad (3)$$

where the vector $\mathbf{h}_{i,k} \in \mathbb{C}^{N_t}$ denotes the frequency domain channel between the BS and the k -th user, and the scalar $z_{i,k} \in \mathcal{CN}(0, \sigma_c^2)$ denotes the additive white Gaussian noise (AWGN). In order to achieve satisfactory multi-user communication performance, the precoders \mathbf{W}_i should be properly designed to suppress multi-user interference and improve information transmission rate. While the precoder/beamforming design for ISAC systems has been extensively investigated [3]–[5], in this paper we focus on the radar echo signal processing method to provide satisfactory parameter estimation performance based on OFDM communication waveforms.

C. Sensing Signal Model

From the radar sensing perspective, the dual-functional BS attempts to estimate the angle-range-velocity information of multiple point-like targets by processing the received echo signals. We assume that there are Q targets within the areas of interest, in which the angle-range-velocity information of the q -th target is denoted as θ_q , d_q , and v_q , respectively, $q \in \mathcal{Q} \triangleq \{1, \dots, Q\}$. It is noted that the direction of arrival (DoA) and the direction of departure (DoD) are the same as θ_q in the considered mono-static ISAC system.

The transmitted OFDM signals will reach the Q targets and be reflected back to the receive antennas of the BS. In specific, the transmitted OFDM signals will experience round-trip path-loss and propagation delay, and the Doppler frequency shift before arriving at the receive antenna array. Thus, the baseband echo signal received by the m -th antenna on the i -th subcarrier can be expressed as

$$\begin{aligned} \tilde{y}(m, i, t) \triangleq & \sum_{q=1}^Q \beta_q \sqrt{\text{PL}(2d_q)} \sum_{n=0}^{N_t-1} [\tilde{x}(n, i, t - 2d_q/c) \\ & e^{-j2\pi n d_t \sin \theta_q / \lambda_c} e^{-j2\pi m d_r \sin \theta_q / \lambda_c} e^{j2\pi f_{D,q} t}] \\ & + \tilde{z}(m, i, t), \end{aligned} \quad (4)$$

where $m = 0, \dots, N_r - 1$ is the index of receive antennas, the scalar β_q denotes the reflection coefficient of the q -th target with power $\mathbb{E}\{|\beta_q|^2\} = \sigma_\beta^2$, the scalar $\text{PL}(d) \triangleq c_0(d/d_0)^{-\alpha}$ represents the distance-dependent path-loss with c_0 being the loss at the reference distance d_0 , d the link distance and α the path-loss exponent, the scalar d_t is the transmit antenna spacing, the scalar d_r is the receive antenna spacing, $f_{D,q} \triangleq 2v_q f_c / c$ is the Doppler frequency of the q -th target, and the scalar $\tilde{z}(m, i, t)$ is the independently and identically distributed (i.i.d.) AWGN at the receive antennas. It is generally assumed that the channel scattering coefficients, the reflection coefficients and the angle-range-velocity of targets are constant during one CPI. Considering that the signal

bandwidth is usually much smaller than the central carrier frequency, the phase shifts along the spatial axis are assumed to be identical on all subcarriers and the Doppler frequency shift within one OFDM symbol is also assumed to be identical on all subcarriers. In addition, we note that only the first-order reflection from the target is considered due to high attenuation.

As presented in Fig. 1, the received echo signals (4) are processed by ADCs with the sampling frequency $F_s \triangleq N_s \Delta f$ and removing CP. Then, according to the expression of transmitted signal in (2), the digital baseband echo signals can be written as

$$\begin{aligned} \tilde{y}(m, i, lT + \tau) \triangleq & \sum_{q=1}^Q \beta_q \sqrt{\text{PL}(2d_q)} \sum_{n=0}^{N_t-1} [x(n, i, l) \\ & e^{j2\pi i \Delta f (lT + \tau - 2d_q/c)} e^{-j2\pi n d_t \sin \theta_q / \lambda_c} \\ & e^{-j2\pi m d_r \sin \theta_q / \lambda_c} e^{j2\pi f_{D,q} (lT + \tau)}] \\ & + \tilde{z}(m, i, lT + \tau), \quad \forall l, \tau \in [0, T_d]. \end{aligned} \quad (5)$$

Finally, by applying an N_s -point DFT, the echo signal received by the m -th receive antenna on the i -th subcarrier can be formulated as

$$\begin{aligned} y(m, i, l) \triangleq & \sum_{q=1}^Q \beta_q \sqrt{\text{PL}(2d_q)} \mathbf{a}^H(\omega_t(\theta_q)) \mathbf{x}_i[l] \\ & e^{jm\omega_r(\theta_q)} e^{jn\omega_d(d_q)} e^{jl\omega_v(v_q)} + z(m, i, l), \end{aligned} \quad (6)$$

where $z(m, i, l) \sim \mathcal{CN}(0, \sigma_z^2)$ denotes the DFT of the AWGN $\tilde{z}(m, i, lT + \tau)$ during the l -th OFDM symbol. For conciseness, in (6) we respectively define the transmit steering vector $\mathbf{a}(\omega)$, and the digital frequencies related to the DoD with respect to transmit antennas, the DoA with respect to receive antennas, the range and the velocity of the q -th target as

$$\mathbf{a}(\omega) \triangleq [e^{j0}, e^{j1\omega}, \dots, e^{j(N_t-1)\omega}]^T, \quad (7a)$$

$$\omega_t(\theta_q) \triangleq 2\pi d_t \sin \theta_q / \lambda_c, \quad (7b)$$

$$\omega_r(\theta_q) \triangleq -2\pi d_r \sin \theta_q / \lambda_c, \quad (7c)$$

$$\omega_d(d_q) \triangleq -4\pi \Delta f d_q / c, \quad (7d)$$

$$\omega_v(v_q) \triangleq 4\pi T v_q f_c / c. \quad (7e)$$

For radar sensing functionality, in this paper we focus on estimating the angle-range-velocity information of the targets based on the received echo signal $y(m, i, l)$ in (6). The angle θ_q , the range d_q , and the velocity v_q of the targets are determined by the digital frequencies $\omega_r(\theta_q)$, $\omega_d(d_q)$, and $\omega_v(v_q)$, respectively. We note that radar target parameter estimation is performed during one CPI using the data cube of received echo signals as modeled in (6), which can be visually illustrated as in Fig. 3. It is clear that the data cube consists of three dimensions, i.e., the spatial-delay-Doppler dimensions that are related to the receive antennas, the carriers, and the OFDM symbols, respectively, from which we attempt to extract the angle-range-velocity information of potential targets. However, we observe that the sinusoidal functions with angle/range/velocity-dependent digital frequencies are multiplied by the signal-dependent coefficients $\mathbf{a}^H(\omega_t(\theta_q)) \mathbf{x}_i[l]$, which are determined by the transmitted dual-functional signals and the DoDs of potential targets. Therefore, the angle-

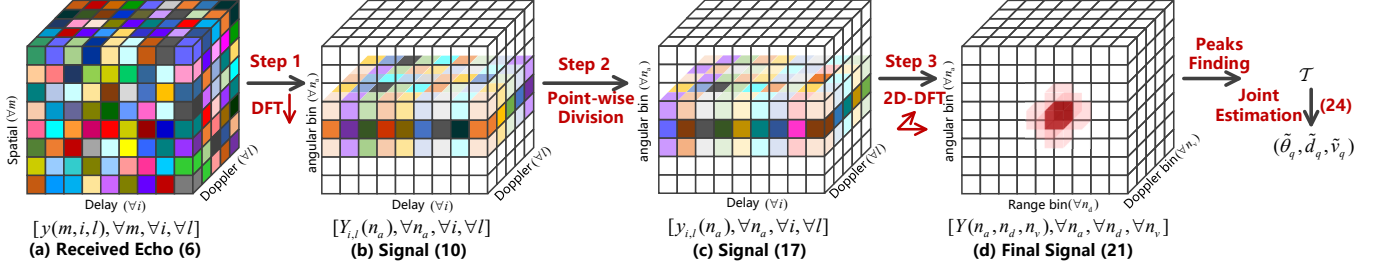


Fig. 3: The processing flowchart of the proposed joint estimation method.

range-velocity information cannot be directly extracted from the data cube via typical spectrum analysis. In order to tackle this difficulty, we propose a novel joint angle-range-velocity estimation method to remove the influence of the signal-dependent coefficients and fully exploit the data cube to improve the parameter estimation performance.

III. JOINT ANGLE-RANGE-VELOCITY ESTIMATION

In this section, we focus on extracting the angle-range-velocity information of potential targets from the received echo signals $y(m, i, l)$, $\forall m, \forall i, \forall l$. A novel joint estimation method is proposed to fully exploit the data cube during one CPI and jointly estimate the angle-range-velocity information.

A. Observations from the Echo Signals

To achieve better parameter estimation performance, we specifically examine the received echo signals $y(m, i, l)$ and its representation in Fig. 3. According to the signal model in (6), we have the following observations

- Along the spatial dimension (i.e., along the axis of receive antennas $\{m = 0, 1, \dots, N_r - 1\}$), the echo signals can be regarded as the summation of Q sinusoidal functions with the digital frequency being determined by the DoA θ_q and the constant amplitude.
- Along the delay dimension (i.e., along the axis of carriers $\{i = 0, 1, \dots, N_s - 1\}$), the echo signals are composed of Q sinusoidal functions multiplied by different coefficients. Particularly, the digital frequencies along the delay dimension are determined by the range of potential target d_q and the signal-dependent coefficient $\mathbf{a}^H(\omega_t(\theta_q)) \mathbf{x}_i[l]$.
- Along the Doppler dimension (i.e., along the axis of symbols $\{l = 0, 1, \dots, L - 1\}$), the echo signals also consist of Q sinusoidal functions multiplied by different signal-dependent coefficients. In other words, the digital frequencies along the Doppler dimension are determined by the velocity of potential target v_q and the signal-dependent coefficient $\mathbf{a}^H(\omega_t(\theta_q)) \mathbf{x}_i[l]$.
- As for the signal-dependent coefficient $\mathbf{a}^H(\omega_t(\theta_q)) \mathbf{x}_i[l]$, it is related to the DoD of potential target θ_q to be estimated and the transmitted signal $\mathbf{x}_i[l]$. As presented in (1), the dual-functional transmitted signal $\mathbf{x}_i[l]$ is a function of transmitted communication symbols, which are randomly generated. Therefore, the signal-dependent coefficient $\mathbf{a}^H(\omega_t(\theta_q)) \mathbf{x}_i[l]$ will significantly influence

the spectrum analysis for estimating the angle-range-velocity information of potential targets.

Based on above observations, it is clear that the angle-range-velocity information is fused in different dimensions of the data cube. Moreover, the signal-dependent coefficient $\mathbf{a}^H(\omega_t(\theta_q)) \mathbf{x}_i[l]$ is the major difficulty in extracting target parameters. Therefore, in order to improve parameter estimation performance, we propose a novel joint estimation method to remove the signal-dependent coefficients and jointly estimate the target parameters based on the data cube. The details are presented as follows.

B. Step 1: Spectrum Analysis along the Spatial Dimension

Considering that the digital frequencies of echo signals along the spatial dimension are determined by θ_q and the signal-dependent coefficient $\mathbf{a}^H(\omega_t(\theta_q)) \mathbf{x}_i[l]$ is also related to θ_q , we first analyze the spectrum of echo signals along the spatial dimension to present its characteristics in different angular bins.

In order to perform spectrum analysis along the spatial dimension, the echo signal (6) is re-arranged as

$$y(m, i, l) = \sum_{q=1}^Q \mathcal{A}(q, i, l) e^{jm\omega_r(\theta_q)} + z(m, i, l), \quad (8)$$

where $\mathcal{A}(q, i, l)$ is constant along the spatial dimension and defined as

$$\mathcal{A}(q, i, l) \triangleq \beta_q \sqrt{\text{PL}(2d_q)} \mathbf{a}^H(\omega_t(\theta_q)) \mathbf{x}_i[l] e^{jl\omega_d(d_q)} e^{jl\omega_v(v_q)}. \quad (9)$$

It is clear that each sequence along the spatial dimension, i.e., $\{y(m, i, l), m = 0, \dots, N_r - 1\}$, $\forall i, \forall l$, can be viewed as a sum of the noise and Q sinusoidal functions with the angle-dependent digital frequency $\omega_r(\theta_q)$ and the amplitude $\mathcal{A}(q, i, l)$. Thus, through spectrum analysis algorithms, we can easily obtain the DoAs of potential targets. However, it is unwise to estimate the angles θ_q by utilizing only one sequence $\{y(m, i, l), m = 0, \dots, N_r - 1\}$ [35] instead of the whole data cube $\{y(m, i, l), m = 0, \dots, N_r - 1, \forall i, \forall l\}$, since the latter enables larger processing gains. Moreover, although the estimated angle information can be utilized to remove the signal-dependent coefficient $\mathbf{a}^H(\omega_t(\theta_q)) \mathbf{x}_i[l]$, the estimation error in the spatial dimension will be propagated and even amplified to the estimation process for other parameters, which may result in deteriorating target estimation performance. Therefore, instead of estimating θ_q , here the main purpose

of spectrum analysis along the spatial dimension is to capture the characteristics of echo signals in different angular bins.

The spectrum analysis for $\{y(m, i, l), m = 0, \dots, N_r - 1\}$, $\forall i, \forall l$ can be conducted by various algorithms, e.g., DFT [39], MUSIC [40], ESPRIT [41], compressed sensing based methods [13], [14]. In the rest of this paper, we use the typical DFT algorithm without loss of generality to explicitly present the mathematics and advantages of the proposed algorithm. In particular, by applying an N_a -point normalized DFT, $N_a \geq N_r$, we can extract the characteristics of the echo signals in different angular bins and obtain the sequences $\{Y_{i,l}(n_a), n_a = -\lfloor N_a/2 \rfloor, \dots, \lfloor N_a/2 \rfloor - 1\}$, $\forall i, \forall l$, with $Y_{i,l}(n_a)$ being written as

$$Y_{i,l}(n_a) \triangleq \frac{1}{N_r} \sum_{m=0}^{N_r-1} y(m, i, l) e^{-jm\tilde{\omega}_r(n_a)}, \quad (10)$$

where the n_a -th frequency component ranging from $-\pi$ to π is defined as

$$\tilde{\omega}_r(n_a) \triangleq \frac{2\pi n_a}{N_a}. \quad (11)$$

Since a larger N_a means more angular bins, better angle estimation performance will be achieved with a larger N_a [39], [42], which requires zero-padding operation before DFT. Meanwhile, considering that the computational complexity of DFT increases with N_a , a proper value is advocated to achieve a satisfactory trade-off between estimation performance and computational complexity. Through spectrum analysis along the spatial dimension, the echo signals $\{y(m, i, l), m = 0, 1, \dots, N_r - 1\}$ are converted into N_a components, each of which has a single digital frequency $\tilde{\omega}_r(n_a)$ and a complex amplitude $Y_{i,l}(n_a)$, i.e.,

$$y(m, i, l) = \sum_{n_a=-\lfloor N_a/2 \rfloor}^{\lfloor N_a/2 \rfloor - 1} Y_{i,l}(n_a) e^{jm\tilde{\omega}_r(n_a)}. \quad (12)$$

Moreover, according to the expression of $y(m, i, l)$ in (8), the signal power along the spatial dimension after DFT operation will be concentrated on several angular bins related to the DoAs of potential targets, as shown in Fig. 3b. Specifically, the power of the n_a -th angular bin is $|Y_{i,l}(n_a)|^2$, which indicates the probability of the existence of the targets whose angle-dependent digital frequencies $\omega_r(\theta_q)$ approximates to $\tilde{\omega}_r(n_a)$. Next, we will utilize this characteristic to facilitate the following range and velocity estimation.

For the following range and velocity estimation, we denote the index set of the targets whose DoAs are within the n_a -th angular bin as \mathcal{Q}_{n_a} with the cardinality being $|\mathcal{Q}_{n_a}| = Q_{n_a}$. It is obvious that $\mathcal{Q}_{n_a} \subseteq \mathcal{Q}$, $0 \leq Q_{n_a} \leq Q$, $\mathcal{Q}_{n_a} \cap \mathcal{Q}_{n'_a} = \emptyset$, $\forall n_a \neq n'_a$, and $\sum_{n_a} \mathcal{Q}_{n_a} = \mathcal{Q}$. For the DoAs within the n_a -th angular bin, we have the following approximation

$$\omega_r(\theta_q) \approx \tilde{\omega}_r(n_a), \quad \forall q \in \mathcal{Q}_{n_a}. \quad (13)$$

Then, substituting the expression of $y(m, i, l)$ in (8) and the approximation in (13) into (10), the amplitude of the n_a -th angular bin can be approximated as

$$Y_{i,l}(n_a) \approx \sum_{q \in \mathcal{Q}_{n_a}} \mathcal{A}(q, i, l), \quad (14)$$

where the noise component is ignored in order to focus on extracting desired parameters from the target echo signals. With expression (9), we observe that $Y_{i,l}(n_a)$ consists of Q_{n_a} components, each of which is the signal-dependent coefficient $\mathbf{a}^H(\omega_r(\theta_q))\mathbf{x}_i[l]$ multiplied by the sinusoidal functions whose digital frequencies are related to the range and velocity of potential targets. Since the signal-dependent coefficient changes along the delay and Doppler dimensions, it hinders the estimation of range and velocity using spectrum analysis algorithms. Thus, the next step is to eliminate the impact of the signal-dependent coefficient on the spectrum analysis along the delay and Doppler dimensions.

C. Step 2: Signal-Dependent Coefficients Removing

After spectrum analysis along the spatial dimension, the amplitude of the echo signals with different angle-dependent frequencies are extracted and reserved in different angular bins. Then, the signal-dependent coefficient $\mathbf{a}^H(\omega_r(\theta_q))\mathbf{x}_i[l]$ must be removed to eliminate its influence on the spectrum analysis along the delay and Doppler dimensions before jointly estimating the angle-range-velocity information. We note that the transmitted signals $\mathbf{x}_i[l]$ are known at the dual-functional BS, however, the DoAs of potential targets θ_q are the parameters to be estimated. In order to remove the signal-dependent coefficient, the authors in [35] proposed to first estimate the DoAs θ_q through spectrum analysis along the spatial dimension, and then use the obtained results to directly divide it. Nevertheless, using the sequence on one subcarrier and during one OFDM symbol to estimate the DoAs is not efficient and may cause estimation error. For the purpose of improving the joint estimation performance and avoiding the angular estimation error propagation, we propose to remove the signal-dependent coefficient for each angular bin respectively, instead of only focusing on few estimated angular bins related to potential targets.

In specific, for the targets in the n_a -th angular bin, the digital frequency related to the DoAs $\omega_r(\theta_q)$ is approximated by $\tilde{\omega}_r(n_a)$. According to the definitions of $\omega_r(\theta_q)$ in (7c) and the digital frequency related to the DoDs $\omega_t(\theta_q)$ in (7b), we can acquire

$$\omega_t(\theta_q) \approx (-d_t/d_r)\tilde{\omega}_r(n_a), \quad \forall q \in \mathcal{Q}_{n_a}. \quad (15)$$

Then, substituting (15) and the definition of $\mathcal{A}(q, i, l)$ in (9) into (14), the amplitude of the n_a -th angular bin can be rewritten as

$$Y_{i,l}(n_a) \approx \sum_{q \in \mathcal{Q}_{n_a}} \beta_q \sqrt{\text{PL}(2d_q)} \mathbf{a}^H((-d_t/d_r)\tilde{\omega}_r(n_a))\mathbf{x}_i[l] e^{j\omega_d(d_q)} e^{j\omega_v(v_q)}. \quad (16)$$

From above equation, we observe that the signal-dependent coefficient $\mathbf{a}^H(\omega_t(\theta_q))\mathbf{x}_i[l]$ is converted into a known component at the BS, i.e., $\mathbf{a}^H((-d_t/d_r)\tilde{\omega}_r(n_a))\mathbf{x}_i[l]$, which can be directly removed via point-wise division. However, since the magnitudes of the signal-dependent coefficients are not identical for different angular bins, directly dividing $Y_{i,l}(n_a)$ by the signal-dependent coefficient will destroy the characteristics of echo signals in the spatial dimension. In other words,

the spatial characteristics of echo signals is changed after dividing $Y_{i,l}(n_a)$, $\forall n_a$ by different values, which will lead to deteriorate angular estimation performance once the peaks of these angular bins are different. Thus, in an effort to eliminate the impact of the signal-dependent coefficient, we should also maintain the spatial characteristics of echo signals, i.e., not change the relationship between the powers of different angular bins. For this purpose, we introduce a scaling factor α_{n_a} for the n_a -th angular bin and propose to divide $Y_{i,l}(n_a)$ by the product of α_{n_a} and the signal-dependent coefficient $\mathbf{a}^H((-d_t/d_r)\tilde{\omega}_r(n_a))\mathbf{x}_i[l]$. The result after eliminating the impact of signal-dependent coefficients can thus be expressed as

$$y_{i,l}(n_a) \triangleq \frac{Y_{i,l}(n_a)}{\alpha_{n_a} \mathbf{a}^H((-d_t/d_r)\tilde{\omega}_r(n_a))\mathbf{x}_i[l]}. \quad (17)$$

Then, based on above discussions, the scaling factor α_{n_a} should be chosen to preserve the power of the n_a -th angular bin unchanged, i.e., the power of the sequence after division $y_{i,l}(n_a)$ maintains the same as that of the original sequence $Y_{i,l}(n_a)$:

$$\sum_{i,l} |y_{i,l}(n_a)|^2 = \sum_{i,l} |Y_{i,l}(n_a)|^2, \quad \forall n_a, \quad (18)$$

with which the scaling factor α_{n_a} can be calculated as

$$\alpha_{n_a} = \sqrt{\frac{\sum_{i,l} \left| \frac{Y_{i,l}(n_a)}{\mathbf{a}^H((-d_t/d_r)\tilde{\omega}_r(n_a))\mathbf{x}_i[l]} \right|^2}{\sum_{i,l} |Y_{i,l}(n_a)|^2}}. \quad (19)$$

According to (16) and (17), the sequences after removing the signal-dependent coefficients can be expressed as

$$y_{i,l}(n_a) \approx \sum_{q \in \mathcal{Q}_{n_a}} \beta_q \sqrt{\text{PL}(2d_q)/\alpha_{n_a}} e^{j\omega_d(d_q)} e^{j\omega_v(v_q)}. \quad (20)$$

Now we clearly see that the sequence $\{y_{i,l}(n_a), \forall i\}$ or $\{y_{i,l}(n_a), \forall l\}$ is composed of Q_{n_a} sinusoidal functions whose digital frequencies are determined by the range d_q or the velocity v_q of the target. Therefore, it is easy to conduct spectrum analysis along the delay and Doppler dimensions and then jointly estimate the desired angle-range-velocity information, which is presented in the next subsection.

D. Step 3: Spectrum Analysis along the Delay and Doppler Dimensions and Joint Estimation

Given the sequence $y_{i,l}(n_a)$, $\forall n_a, \forall i, \forall l$ in (20), the angle-range-velocity information of potential targets can be jointly extracted via spectrum analysis. For the sequences in the n_a -th angular bin, we observe that the result $y_{i,l}(n_a)$ is composed of Q_{n_a} sinusoidal functions with the range-dependent frequency $\omega_d(d_q)$ and the velocity-dependent frequency $\omega_v(v_q)$ along the delay and Doppler dimensions, respectively. Therefore, a 2-dimensional DFT operation is employed along these two dimensions to extract the characteristics of echo signals in different range and Doppler bins.

Specifically, the normalized (N_d, N_v) -point 2D-DFT ($N_d \geq N_s$, $N_v \geq L$) is implemented on the obtained sequences $\{y_{i,l}(n_a), \forall i, \forall l\}$, $\forall n_a$, and yields the sequences $\{Y(n_a, n_d, n_v), n_d = -N_d + 1, \dots, 0, n_v =$

$-[N_v/2], \dots, [N_v/2] - 1\}$, $\forall n_a$, in which the amplitude $Y(n_a, n_d, n_v)$ can be calculated as

$$Y(n_a, n_d, n_v) \triangleq \frac{1}{N_s L} \sum_{i=0}^{N_s-1} \sum_{l=0}^{L-1} y_{i,l}(n_a) e^{-j l \tilde{\omega}_v(n_v)} e^{-j i \tilde{\omega}_d(n_d)}. \quad (21)$$

The frequency components of the k_v -th Doppler bin and the k_d -th range bin are respectively defined as

$$\tilde{\omega}_v(k_v) \triangleq \frac{2\pi k_v}{N_v}, \quad (22a)$$

$$\tilde{\omega}_d(k_d) \triangleq \frac{2\pi k_d}{N_d}. \quad (22b)$$

After obtaining the amplitude $Y(n_a, n_d, n_v)$ for each of the $N_a \times N_d \times N_v$ angular-range-Doppler bins, we can jointly estimate the targets from these three dimensions. In particular, the angle-range-velocity information of the Q targets is jointly estimated by finding the peaks of the obtained three-dimensional signals, i.e.,

$$\mathcal{T} \triangleq \{\mathcal{T}_1, \dots, \mathcal{T}_Q\} = \mathcal{P}_3\{Y(n_a, n_d, n_v), \forall n_a, \forall n_d, \forall n_v\}, \quad (23)$$

where $\mathcal{P}_3\{\cdot\}$ outputs the indices of the peaks of the input three-dimensional sequence and the set \mathcal{T}_q contains the indices of the angular-range-Doppler bins for the q -th peak. Then, the estimated angle-range-velocity of the q -th target, i.e., $\hat{\theta}_q, \hat{d}_q, \hat{v}_q$, can be recovered by using the three-dimensional index $\mathcal{T}_q = \{(n_a, n_d, n_v)\}$ as

$$\hat{\theta}_q = \arcsin\left(-\frac{n_a \lambda_c}{d_r N_a}\right), \quad (24a)$$

$$\hat{d}_q = -\frac{cn_d}{2N_d \Delta f}, \quad (24b)$$

$$\hat{v}_q = \frac{cn_v}{2N_v T f_c}. \quad (24c)$$

It should be emphasized that the angle-range-velocity information is jointly estimated via finding peaks in the three-dimensional space. Compared with the existing approaches that successively estimate angle/range/velocity along the corresponding dimension, the proposed algorithm achieves better parameter estimation performance especially when the targets are relatively close along a certain dimension. This is because the proposed algorithm estimates the target from three dimensions, as illustrated in Fig. 3d, instead of determining the target from one dimension.

E. Summary of the Joint Estimation Algorithm

Based on the above descriptions, the proposed joint angle-range-velocity estimation approach is straightforward and summarized in Algorithm 1. In summary, the spectrum analysis along the spatial dimension is first performed to extract the characteristics of echo signals in different angular bins, then the scaling factor is introduced to assist to remove the signal-dependent coefficient for each angular bin without destroying the spatial characteristics of echo signals, and after applying a 2-dimensional DFT along the delay and Doppler dimensions, the angle-range-velocity information is jointly estimated via finding peaks among the obtained three-dimensional sequence.

Algorithm 1 The Proposed Joint Angle-Range-Velocity Estimation Approach

Input: $\{y(m, i, l), \forall m, \forall i, \forall l\}$, $N_t, N_r, N_s, L, N_a, N_d, N_v, d_t, d_r, \lambda_c, c, f_c, T, \Delta f, \mathbf{x}_i[l], \forall i, \forall l$.

Output: θ_q, d_q, v_q .

- 1: Perform N_a -point DFT along the spatial dimension to obtain $Y_{i,l}(n_a), \forall i, \forall l, n_a = -\lfloor N_a/2 \rfloor, \dots, \lfloor N_a/2 \rfloor - 1$ in (10).
 - 2: Calculate scaling factor α_{n_a} in (19).
 - 3: Remove signal-dependent coefficients to obtain $y_{i,l}(n_a)$ in (17).
 - 4: Perform 2-D DFT along the delay and Doppler dimensions to obtain $Y(n_a, n_d, n_v)$ in (21).
 - 5: Find the peaks of $\{Y(n_a, n_d, n_v), \forall n_a, \forall n_d, \forall n_v\}$ to obtain the index set \mathcal{T} .
 - 6: Recover the estimated $\tilde{\theta}_q, \tilde{d}_q$, and \tilde{v}_q by (24).
 - 7: Return $\theta_q = \tilde{\theta}_q, d_q = \tilde{d}_q$, and $v_q = \tilde{v}_q$.
-

IV. PERFORMANCE ANALYSIS

Based on the above developments, in this section we conduct theoretical analysis to evaluate the performance of the proposed joint estimation algorithm. In particular, we derive the achievable maximum unambiguous range and resolution of parameter estimation, which are two key performance indicators generally considered in traditional radar systems, and the processing gain that represents the ability against noise.

A. Maximum Unambiguous Range

Owing to the well-known 2π periodicity of the digital frequency, two frequencies whose values differ by $2\pi z, z \in \mathbb{Z}$, will be estimated to be the same value through spectrum analysis. Therefore, the digital frequencies related to the angle-range-velocity information should satisfy the following relationship to avoid ambiguity

$$-\pi \leq \omega_r(\theta) \leq \pi, \quad (25a)$$

$$-2\pi \leq \omega_d(d) \leq 0, \quad (25b)$$

$$-\pi \leq \omega_v(v) \leq \pi. \quad (25c)$$

Then, according to the definitions of digital frequencies in (7), the maximum unambiguous range of the angle, range, and velocity can be respectively calculated as

$$\theta_{\max} \triangleq \arcsin(\lambda_c/2d_r), \quad (26a)$$

$$d_{\max} \triangleq \frac{c}{2\Delta f}, \quad (26b)$$

$$v_{\max} \triangleq \frac{c}{4Tf_c}. \quad (26c)$$

We can observe that the maximum unambiguous range is determined by the wavelength, the antenna spacing, the frequency spacing, the symbol duration, and the carrier frequency, while is irrelevant to the transmit antenna array, the transmit power budget and the signal processing algorithms.

B. Resolution

We note that the proposed joint estimation algorithm estimates the targets by distinguishing the angular-range-Doppler

bins. Considering that the angular-range-Doppler bins are formulated by performing DFT in this paper, the resolution is also determined by the DFT theory [39]. In specific, the frequency resolution for an N -point DFT without zero-padding equals to $2\pi/N$. In addition, the zero-padding operation does not influence the frequency resolution. Thus, according to the definitions of the digital frequencies in (7), the resolution along the spatial dimension Δ_a , the delay dimension Δ_d , and the Doppler dimension Δ_v , respectively, satisfy

$$\omega_r(\theta + \Delta_a) - \omega_r(\theta) = 2\pi/N_r, \quad (27a)$$

$$\omega_d(d + \Delta_d) - \omega_d(d) = 2\pi/N_s, \quad (27b)$$

$$\omega_v(v + \Delta_v) - \omega_v(v) = 2\pi/L, \quad (27c)$$

which results in

$$\Delta_a \triangleq \frac{\lambda_c}{N_r d_r}, \quad (28a)$$

$$\Delta_d \triangleq \frac{c}{2N_s \Delta f}, \quad (28b)$$

$$\Delta_v \triangleq \frac{c}{2f_c L T}. \quad (28c)$$

Since the proposed algorithm jointly utilizes DFT along the spatial-delay-Doppler dimensions, the targets can be separated when any one of the resolution requirement is satisfied. While for the existing approach that successively estimates the angle-range-velocity information, the angular resolution must be satisfied in order to successfully separate two different targets. Therefore, it is obvious that the proposed joint estimation algorithm can greatly improve the parameter estimation performance in terms of resolution.

C. Processing Gain

In addition to the typical metrics of maximum unambiguous range and resolution, the output SNR and processing gain are also vital for evaluating the parameter estimation performance and the advantages of the proposed estimation algorithm. In other words, a larger output SNR or processing gain indicates stronger abilities against noise and lower estimation errors.

Based on the received echo signal model in (6), the SNR of the received echo signals from the q -th target during one CPI can be calculated as

$$\text{SNR}_{r,q} \triangleq \mathbb{E} \left\{ \sum_{m,i,l} |\beta_q \sqrt{\text{PL}(2d_q)} \mathbf{a}^H(\omega_t(\theta_q)) \mathbf{x}_i[l]|^2 \right\} / \mathbb{E} \left\{ \sum_{m,i,l} |z(m, i, l)|^2 \right\} \quad (29a)$$

$$= \frac{\sigma_\beta^2 \text{PL}(2d_q) \mathbb{E} \left\{ \sum_{m,i,l} |\mathbf{a}^H(\omega_t(\theta_q)) \mathbf{x}_i[l]|^2 \right\}}{N_r N_s L \sigma_z^2} \quad (29b)$$

$$= \frac{\sigma_\beta^2 \text{PL}(2d_q) \sum_{i,l} |\mathbf{a}^H(\omega_t(\theta_q)) \mathbf{x}_i[l]|^2}{N_s L \sigma_z^2}. \quad (29c)$$

Then, we derive the output SNR of the proposed joint estimation algorithm for estimating the q -th target. In particular, assuming that the q -th target is estimated to be in the (n_a, n_d, n_v) -th angular-range-Doppler bin, i.e., $(\omega_r(\theta_q), \omega_d(d_q), \omega_v(v_q)) \approx (\tilde{\omega}_r(n_a), \tilde{\omega}_d(n_d), \tilde{\omega}_v(n_v))$, the

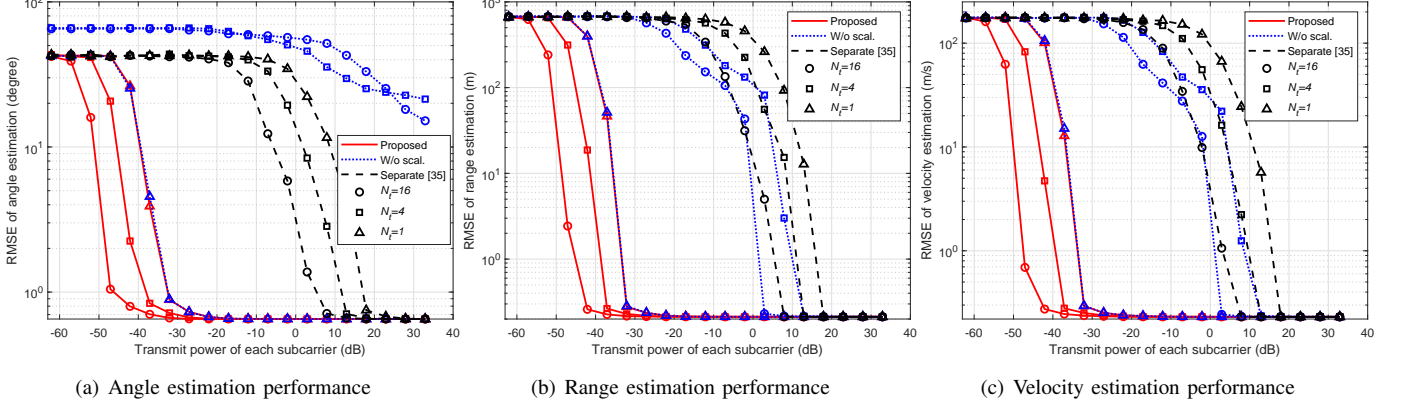


Fig. 4: Estimation performance versus transmit power with different transmit antennas, $N_t = 1, 4, 16$.

amplitude $Y(n_a, n_d, n_v)$ in this angular-range-Doppler bin can be calculated by substituting (20) into (21) as

$$Y(n_a, n_d, n_v) \approx \beta_q \sqrt{\text{PL}(2d_q)} / \alpha_{n_a}. \quad (30)$$

Meanwhile, by using the same procedure as that for processing the target echo signals in (10), (17) and (21), the amplitude $Z(n_a, n_d, n_v)$ corresponding to the received AWGN $z(m, i, l)$ is given by

$$Z(n_a, n_d, n_v) \triangleq \sum_{m,i,l} \frac{z(m, i, l) e^{-jm\tilde{\omega}_r(n_a)} e^{-jl\tilde{\omega}_v(n_v)} e^{-jl\tilde{\omega}_d(n_d)}}{N_r N_s L \alpha_{n_a} \mathbf{a}^H((-d_t/d_r)\tilde{\omega}_r(n_a)) \mathbf{x}_i[l]}, \quad (31)$$

which follows

$$Z(n_a, n_d, n_v) \sim \mathcal{CN}(0, \sigma_{z,n_a}^2), \quad (32)$$

with the noise power of

$$\sigma_{z,n_a}^2 = \sum_{i,l} \frac{\sigma_s^2}{N_r N_s^2 L^2 \alpha_{n_a}^2 |\mathbf{a}^H((-d_t/d_r)\tilde{\omega}_r(n_a)) \mathbf{x}_i[l]|^2}. \quad (33)$$

Thus, the output SNR of the q -th target can be calculated as

$$\text{SNR}_{o,q} \triangleq \frac{\mathbb{E}\{|\beta_q \sqrt{\text{PL}(2d_q)} / \alpha_{n_a}|^2\}}{\sigma_{z,n_a}^2} \quad (34a)$$

$$\approx \frac{N_r N_s^2 L^2 \sigma_\beta^2 \text{PL}(2d_q)}{\sum_{i,l} \sigma_s^2 / |\mathbf{a}^H(\omega_t(\theta_q)) \mathbf{x}_i[l]|^2}, \quad (34b)$$

in which (34b) is obtained due to $\omega_r(\theta_q) \approx \tilde{\omega}_r(n_a)$. Then, the processing gain for estimating the parameters of the q -th target is given by

$$\frac{\text{SNR}_{o,q}}{\text{SNR}_{r,q}} \approx \frac{N_r N_s^3 L^3 / \sum_{i,l} |\mathbf{a}^H(\omega_t(\theta_q)) \mathbf{x}_i[l]|^2}{\sum_{i,l} 1 / |\mathbf{a}^H(\omega_t(\theta_q)) \mathbf{x}_i[l]|^2} \quad (35a)$$

$$\leq N_r N_s L, \quad (35b)$$

where the upper-bound (35b) is derived by using Cauchy-Schwarz inequality. By fully utilizing the $N_r \times N_s \times L$ -dimensional data cube of the received echo signals, we see that the proposed algorithm provides up to $N_r N_s L$ -fold improvement in the received SNR.

TABLE I: System settings.

Parameter	Symbol	Value
Carrier frequency	f_c	28GHz
Subcarrier spacing	Δf	120kHz
Number of subcarriers	N_s	512
OFDM symbol duration	T_d	8.33 μ s
CP duration	T_{cp}	0.59 μ s
Total symbol duration	T	8.92 μ s
Number of OFDM symbols	L	256
Number of transmit antennas	N_t	16
Number of receive antennas	N_r	16
Transmit antenna spacing	d_t	0.5 c/f_c
Receive antenna spacing	d_r	0.5 c/f_c
Reference distance	d_{ref}	1m
Loss of the reference distance	c_{ref}	-30dB
Path loss exponent	α	2.8
Reflection coefficient power	σ_β^2	-10dB
Communication noise power	σ_c^2	-60dBm
Sensing noise power	σ_s^2	-60dBm
QAM order	Ω	16
DFT point in spatial dimension	N_a	$3N_r$
DFT point in delay dimension	N_d	$3N_s$
DFT point in Doppler dimension	N_v	$3L$

V. NUMERICAL RESULTS

In this section, we provide numerical experiments to verify the advantages of the proposed joint estimation method. Unless otherwise specified, we use the settings based on the 3GPP 5G NR high-frequency standard [43], [44], as listed in Table I. In simulations, we assume that the sensing area of interest is known at the BS. Particularly, potential targets are randomly located within the angle of $-30^\circ \sim 30^\circ$, the range of 40m \sim 80m, and the velocity of $-50\text{m/s} \sim 50\text{m/s}$. The transmit beamforming matrix is then designed using the typical zero-forcing scheme [45] to eliminate the multi-user interference and direct the beams towards both the users and potential targets. In addition to the proposed joint estimation algorithm (denoted as ‘‘Proposed’’), we also include two counterparts for comparisons. Specifically, to show the significance of maintaining spatial characteristics by introducing the scaling factor α_{n_a} , we include the joint estimation algorithm without using scaling when removing the signal-dependent coefficients

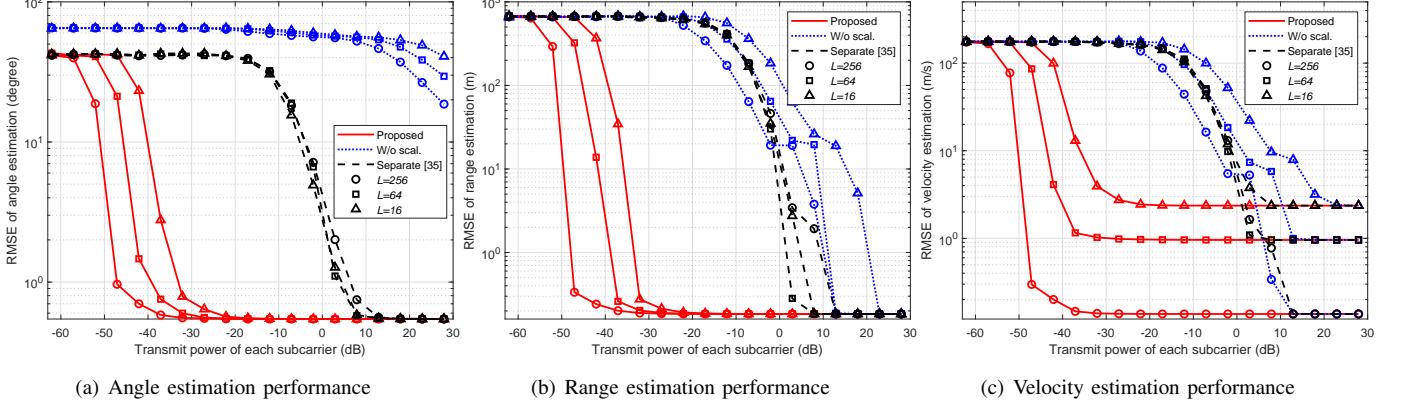


Fig. 5: Estimation performance versus transmit power with different CPI lengths, $L = 16, 64, 256$.

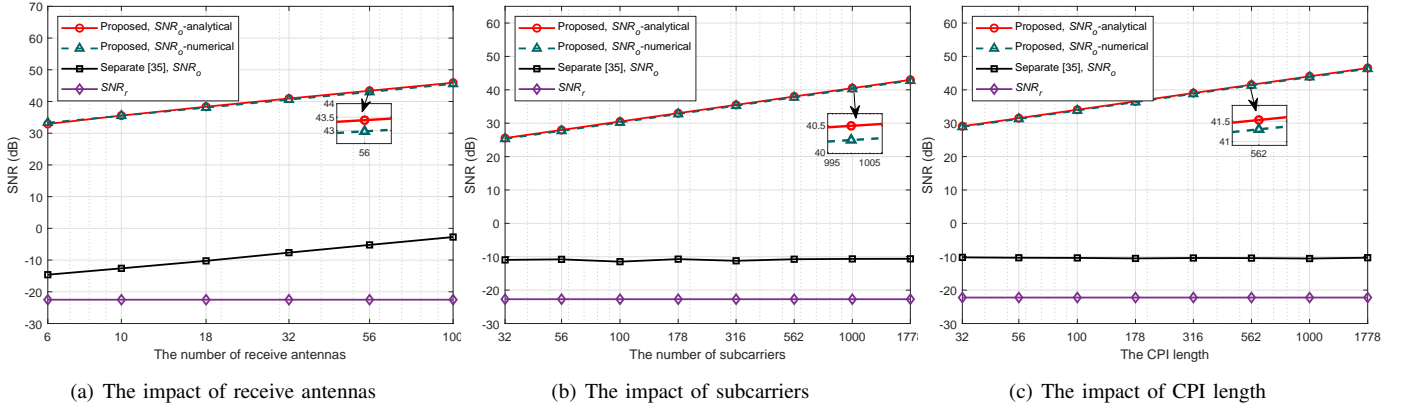


Fig. 6: Received and output SNR versus the number of receive antennas, subcarriers, and CPI lengths, respectively.

(denoted as “W/o scal.”). We also present the existing state-of-the-art algorithm proposed in [35] (denoted as “Separate [35]”), which successively estimates the angle, range, and velocity and only utilizes the echo signals during one OFDM symbol for angle/range estimation. In addition, both the single-target and multi-target scenarios are considered to illustrate the parameter estimation performance. The estimation performance is evaluated in terms of the RMSE of the estimated angle/range/velocity, e.g., the RMSE of the angular estimation is defined as

$$\text{RMSE} = \sqrt{\mathbb{E}\left\{\frac{1}{Q} \sum_{q=1}^Q (\theta_q - \tilde{\theta}_q)^2\right\}}, \quad (36)$$

where θ_q is the actual DoA and $\tilde{\theta}_q$ is the estimated DoA of the q -th target.

A. Single-Target Scenario

To clearly demonstrate the processing gains achieved by fully exploiting the echo signals during one CPI, in this subsection we consider the single-target scenario. We first show the RMSE of angle/range/velocity estimation versus the transmit power in Fig. 4, in which the schemes with different

number of transmit antennas are included. Not surprisingly, the estimation error of all schemes decreases as the transmit power or the number of transmit antennas increases, since more power or a larger transmit antenna array provides higher strength echo signals. In addition, we observe that the RMSE of range/velocity estimation tends to be the same constant value with the increasing of N_t and transmit power. This is because the estimation error is lower bounded by the width of each angular/range/Doppler bin, which is irrelevant to the number of transmit antennas and the transmit power. Meanwhile, since the spatial characteristics of echo signals are destroyed when removing the signal-dependent coefficients, the RMSE of angular estimation achieved by the algorithm without scaling is significantly deteriorated in multi-antenna scenarios. Moreover, the proposed joint estimation algorithm greatly outperforms the successive estimation algorithm proposed in [35], considering that the three-dimensional echo signals are fully exploited to improve the processing gains. This phenomena confirms the advantages of our proposed joint estimation algorithm in MIMO-OFDM ISAC systems.

Then, we show the RMSE performance for the schemes with different CPI lengths in Fig. 5. As already noted, by fully utilizing the received echo signals during one CPI and

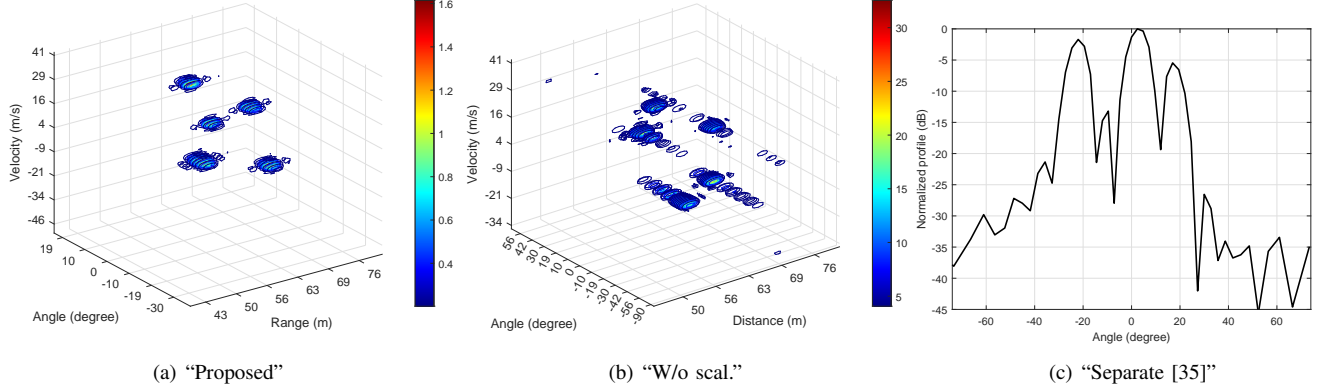


Fig. 7: Radar images of different estimation algorithms.

jointly estimating the parameters through three dimensions, the proposed algorithm achieves the lowest RMSE of angle/range/velocity with a given transmit power. Moreover, compared with the separate estimation algorithm that only utilizes one OFDM symbol for angle/range estimation, the increase of L brings notable performance improvements by using the proposed joint estimation algorithm. In addition, we observe that the RMSE floor of velocity estimation decreases with the increase of $N_v = 3L$, which is consistent with the expression of estimated velocity in (24c).

To further quantify the processing gains of the proposed algorithm, in Fig. 6 we illustrate the SNRs of the received echo signals and the output signals after echo signal processing, i.e., SNR_r in (29) and SNR_o in (34b). The SNRs versus the number of receive antennas, the number of subcarriers, and the CPI length, are shown in Figs. 6(a), (b), and (c), respectively. Both the analytical output SNR as expressed in (34b) and the numerical value, which is calculated as the ratio between the power of the peak in $Y(n_a, n_d, n_v)$ and the noise power, are included. It is observed that the numerical results are almost the same as the theoretical values, which verifies our theoretical analysis. Moreover, we see that the output SNR of our proposed algorithm linearly increases with the number of receive antennas, the number of subcarriers, and the CPI lengths. This is consistent with the expression of SNR_o in (34b) and verifies that the proposed joint estimation algorithm can fully exploit the echo signals from three dimensions. In addition, since the performance of the separate estimation algorithm is determined by the angular estimation, we show the output SNR in extracting the angular information, which obviously only increases with the number of receive antennas. These results reveal that the proposed algorithm that fully utilizes the echo signals to jointly extract the angle-range-velocity has substantially higher processing gains compared with its counterpart, e.g., the proposed algorithm achieves a remarkable SNR processing gain of about 50dB while its counterpart can only provide nearly 10dB.

B. Multi-Target Scenario

In order to illustrate the estimation performance in terms of resolution, in this subsection we consider multi-target

TABLE II: Target parameters

Angle	Range	Velocity
19°	69m	-30m/s
0°	70m	10m/s
5°	60m	25m/s
-25°	50m	30m/s
-20°	65m	-5m/s

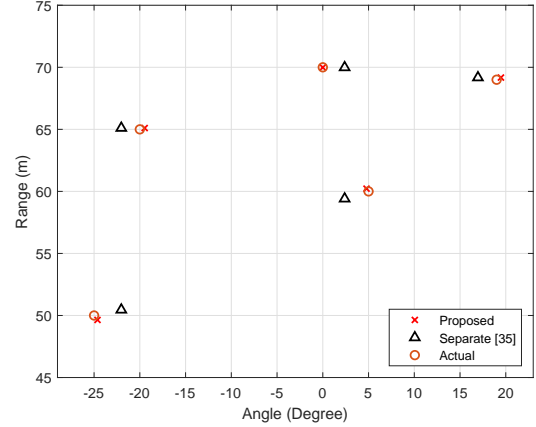


Fig. 8: Target estimation results.

scenarios under the noise-free environment. We assume that there exists $Q = 5$ point-like targets with the angle-range-velocity parameters listed in Table II.

To visually present the parameter estimation performance, we first show the radar images of different algorithms in Fig. 7. We clearly see from Fig. 7(a) that there are five clusters in the radar image corresponding to the five targets by using the proposed estimation algorithm, while the algorithm without scaling in Fig. 7(b) will lead to many wrong peaks along the spatial dimension. Meanwhile, the angle estimation image 7(c) by using the separate estimation algorithm only exhibits three peaks, which indicates that several targets are so close along the spatial dimension that they cannot be distinguished from each other. Thus, there is no doubt that the proposed joint estimation algorithm has better parameter estimation

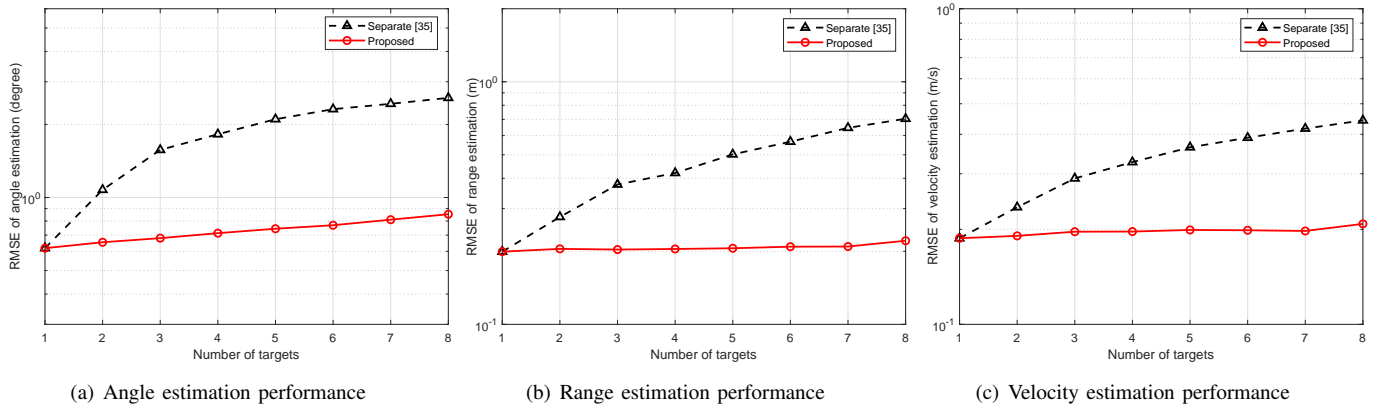


Fig. 9: Estimation performance versus the number of targets.

performance. Based on these radar images, we can obtain the estimation results shown in Fig. 8, in which the true values are marked by orange circles. Since the algorithm without scaling leads to many wrong peaks, we only show the results by using the proposed joint estimation algorithm and the counterpart of separate estimation. It is obvious that the proposed algorithm provides more precise estimation results.

Finally, we present the RMSE of angle/range/velocity estimation versus the number of targets in Fig. 9. It is observed that the performance gap between the proposed joint estimation algorithm and the traditional separate estimation algorithm grows with the number of targets. This phenomenon indicates that by jointly estimating the angle-range-velocity information, the sensing resolution of targets can be improved and better parameter estimation performance is achieved, especially for the scenarios with multiple targets.

VI. CONCLUSIONS

In this paper, we proposed a novel joint estimation algorithm for estimating the parameters of multiple targets based on the MIMO-OFDM waveforms in ISAC systems. We jointly estimated the angle-range-velocity information of potential targets by fully exploiting the received echo signals in a coherent processing interval. Theoretical analysis for the maximum unambiguous range, resolution, and processing gain were provided to evaluate the performance of the proposed echo signal processing algorithm. Extensive simulation results verified that the proposed approach can achieve much better parameter estimation performance compared to existing algorithm. Based on this initial work, we will further investigate transmit beamforming designs and more efficient echo signal processing algorithms for practical applications, in order to achieve a better performance trade-off between multiuser communications and radar target parameter estimation.

REFERENCES

- [1] ITU-R, Report M.2516-0, "Future technology trends of terrestrial international mobile telecommunications systems towards 2030 and beyond," Nov. 2022.
- [2] ITU-R, DRAFT NEW RECOMMENDATION, "Framework and overall objectives of the future development of IMT for 2030 and beyond," Jun. 2023.
- [3] J. A. Zhang, M. L. Rahman, K. Wu, X. Huang, Y. J. Guo, S. Chen, and J. Yuan, "Enabling joint communication and radar sensing in mobile networks - A survey," *IEEE Commun. Surveys Tuts.*, vol. 24, no. 1, pp. 306-345, 1st Quart. 2022.
- [4] F. Liu, Y. Cui, C. Masouros, J. Xu, T. X. Han, Y. C. Eldar, and S. Buzzi, "Integrated sensing and communications: Toward dual-functional wireless networks for 6G and beyond," *IEEE J. Sel. Areas Commun.*, vol. 40, no. 6, pp. 1728-1767, Jun. 2022.
- [5] J. A. Zhang, F. Liu, C. Masouros, R. W. Heath, Z. Feng, L. Zheng, and A. Petropulu, "An overview of signal processing techniques for joint communication and radar sensing," *IEEE J. Sel. Topics Signal Process.*, vol. 15, no. 6, pp. 1295-1315, Nov. 2021.
- [6] Y. Cui, F. Liu, X. Jing, and J. Mu, "Integrating sensing and communications for ubiquitous IoT: Applications, trends, and challenges," *IEEE Netw.*, vol. 35, no. 5, pp. 158-167, Nov. 2021.
- [7] M. Robertson and E. R. Brown, "Integrated radar and communications based on chirped spread-spectrum techniques," in *IEEE MTT-S Int. Microw. Symp. Dig.*, Philadelphia, USA, Jun. 2003, pp. 611-614.
- [8] G. N. Saddik, R. S. Singh, and E. R. Brown, "Ultra-wideband multifunctional communications/radar system," *IEEE Trans. Microw. Theory Techn.*, vol. 55, no. 7, pp. 1431-1437, Jul. 2007.
- [9] K. Wu, J. A. Zhang, X. Huang, Y. J. Guo, and R. W. Heath, "Waveform design and accurate channel estimation for frequency-hopping MIMO radar-based communications," *IEEE Trans. Commun.*, vol. 69, no. 2, pp. 1244-1258, Feb. 2021.
- [10] K. Wu, J. A. Zhang, X. Huang, and Y. J. Guo, "Frequency-hopping MIMO radar-based communications: An overview," *IEEE Aerosp. Electron. Syst. Mag.*, vol. 37, no. 4, pp. 42-54, Apr. 2022.
- [11] P. Kumari, J. Choi, N. G. Prelcic, and R. W. Heath, "IEEE 802.11ad-based radar: An approach to joint vehicular communication-radar system," *IEEE Trans. Veh. Technol.*, vol. 67, no. 4, pp. 3012-3027, Apr. 2018.
- [12] R. C. Daniels, E. R. Yeh, and R. W. Heath, "Forward collision vehicular radar with IEEE 802.11: Feasibility demonstration through measurements," *IEEE Trans. Veh. Technol.*, vol. 67, no. 2, pp. 1404-1416, Feb. 2018.
- [13] M. L. Rahman, J. A. Zhang, X. Huang, Y. J. Guo, and R. W. Heath, "Framework for a perceptive mobile network using joint communication and radar sensing," *IEEE Trans. Aerosp. Electron. Syst.*, vol. 56, no. 3, pp. 1926-1941, Jun. 2020.
- [14] J. A. Zhang, M. L. Rahman, X. Huang, Y. J. Guo, S. Chen, and R. W. Heath, "Perceptive mobile network: Cellular networks with radio vision via joint communication and radar sensing," *IEEE Veh. Technol. Mag.*, vol. 16, no. 2, pp. 20-30, Jun. 2021.
- [15] F. Liu, C. Masouros, A. Li, H. Sun, and L. Hanzo, "MU-MIMO communications with MIMO radar: From co-existence to joint transmission," *IEEE Trans. Wireless Commun.*, vol. 17, no. 4, pp. 2755-2770, Apr. 2018.
- [16] R. Liu, M. Li, Q. Liu, and A. L. Swindlehurst, "Joint waveform and

- filter designs for STAP-SLP-based MIMO-DFRC systems,” *IEEE J. Sel. Areas Commun.*, vol. 40, no. 6, pp. 1918-1931, Jun. 2022.
- [17] R. Liu, M. Li, Y. Liu, Q. Wu, and Q. Liu, “Joint transmit waveform and passive beamforming design for RIS-aided DFRC systems,” *IEEE J. Sel. Topics Signal Process.*, vol. 16, no. 5, pp. 995-1010, Aug. 2022.
 - [18] C.-X. Wang *et al.*, “On the road to 6G: Visions, requirements, key technologies and testbeds,” *IEEE Commun. Surveys Tuts.*, vol. 25, no. 2, pp. 905-974, 2nd Quart. 2023.
 - [19] S. Sen, “OFDM radar space-time adaptive processing by exploiting spatio-temporal sparsity,” *IEEE Trans. Signal Process.*, vol. 61, no. 1, pp. 118-130, Jan. 2013.
 - [20] X. H. Wu, A. A. Kishk, and A. W. Glisson, “MIMO-OFDM radar for direction estimation,” *IET Radar Sonar Navig.*, vol. 4, no. 1, pp. 28-36, Feb. 2010.
 - [21] T. Zhang, X.-G. Xia and L. Kong, “IRCI free range reconstruction for SAR imaging with arbitrary length OFDM pulse,” *IEEE Trans. Signal Process.*, vol. 62, no. 18, pp. 4748-4759, Sep. 2014.
 - [22] X.-G. Xia, T. Zhang, and L. Kong, “MIMO OFDM radar IRCI free range reconstruction with sufficient cyclic prefix,” *IEEE Trans. Aerosp. Electron. Syst.*, vol. 51, no. 3, pp. 2276-2293, Jul. 2015.
 - [23] Y.-H. Cao, X.-G. Xia, and S.-H. Wang, “IRCI free colocated MIMO radar based on sufficient cyclic prefix OFDM waveforms,” *IEEE Trans. Aerosp. Electron. Syst.*, vol. 51, no. 3, pp. 2107-2120, Jul. 2015.
 - [24] C. Sturm and W. Wiesbeck, “Waveform design and signal processing aspects for fusion of wireless communications and radar sensing,” *IEEE Proc.*, vol. 99, no. 7, pp. 1236-1259, Jul. 2011.
 - [25] L. Zheng and X. Wang, “Super-resolution delay-doppler estimation for OFDM passive radar,” *IEEE Trans. Signal Process.*, vol. 65, no. 9, pp. 2197-2210, May 2017.
 - [26] Y. Liu, G. Liao, Y. Chen, J. Xu, and Y. Yin, “Super-resolution range and velocity estimations with OFDM integrated radar and communications waveform,” *IEEE Trans. Veh. Technol.*, vol. 69, no. 10, pp. 11659-11672, Oct. 2020.
 - [27] J. B. Sanson, P. M. Tomé, D. Castanheira, A. Gameiro, and P. P. Monteiro, “High-resolution delay-doppler estimation using received communication signals for OFDM radar-communication system,” *IEEE Trans. Veh. Technol.*, vol. 69, no. 11, pp. 13112-13123, Nov. 2020.
 - [28] Y. Wu, F. Lemic, C. Han, and Z. Chen, “Sensing integrated DFT-Spread OFDM waveform and deep learning-powered receiver design for terahertz integrated sensing and communication systems,” *IEEE Trans. Commun.*, vol. 71, no. 1, pp. 595-610, Jan. 2023.
 - [29] Y. Liu, G. Liao, Z. Yang, and J. Xu, “Multiobjective optimal waveform design for OFDM integrated radar and communication systems,” *Signal Process.*, vol. 141, pp. 331-342, Jun. 2017.
 - [30] Y. Liu, G. Liao, J. Xu, Z. Yang, and Y. Zhang, “Adaptive OFDM integrated radar and communications waveform design based on information theory,” *IEEE Commun. Lett.*, vol. 21, no. 10, pp. 2174-2177, Oct. 2017.
 - [31] M. F. Keskin, V. Koivunen, and H. Wymeersch, “Limited feedforward waveform design for OFDM dual-functional radar-communications,” *IEEE Trans. Signal Process.*, vol. 69, pp. 2955-2970, Apr. 2021.
 - [32] J. Li and P. Stoica, “MIMO radar with colocated antennas,” *IEEE Signal Process. Mag.*, vol. 24, no. 5, pp. 106-114, Sep. 2007.
 - [33] E. Björnson, Y. C. Eldar, E. G. Larsson, A. Lozano, and H. V. Poor, “Twenty-five years of signal processing advances for multiantenna communications: From theory to mainstream technology,” *IEEE Signal Process. Mag.*, vol. 40, no. 4, pp. 107-117, Jun. 2023.
 - [34] Y. Liu, G. Liao, Z. Yang, and J. Xu, “Joint range and angle estimation for an integrated system combining MIMO radar with OFDM communication,” *Multidimensional Syst. Signal Process.*, vol. 30, no. 2, pp. 661-687, 2019.
 - [35] Z. Xu and A. Petropulu, “A bandwidth efficient dual-function radar communication system based on a MIMO radar using OFDM waveforms,” *IEEE Trans. Signal Process.*, vol. 71, pp. 401-416, Feb. 2023.
 - [36] C. B. Barneto, T. Riihonen, M. Turunen, L. Anttila, M. Fleischer, K. Stadius, J. Ryyänänen, and M. Valkama, “Full-duplex OFDM radar with LTE and 5G NR Waveforms: Challenges, solutions, and measurements,” *IEEE Trans. Microw. Theory Techn.*, vol. 67, no. 10, pp. 4042-4054, Oct. 2019.
 - [37] C. B. Barneto, S. D. Liyanaarachchi, M. Heino, T. Riihonen, and M. Valkama, “Full duplex radio/radar technology: The enabler for advanced joint communication and sensing,” *IEEE Wireless Commun.*, vol. 28, no. 1, pp. 82-88, 2021.
 - [38] G. C. Alexandropoulos, M. A. Islam, and B. Smida, “Full-duplex massive multiple-input, multiple-output architectures: Recent advances, applications, and future directions,” *IEEE Veh. Technol. Mag.*, vol. 17, no. 4, pp. 83-91, Dec. 2022.
 - [39] J. G. Proakis, “The discrete Fourier transform: Its properties and applications,” *Digital Signal Processing: Principles, Algorithms and Applications*, 4th ed. Upper Saddle River, N.J.: Pearson Education, 2007, pp. 449-502.
 - [40] R. O. Schmidt, “Multiple emitter location and signal parameter estimation,” *IEEE Trans. Antennas Propagat.*, vol. 34, pp. 276-280, Mar. 1986.
 - [41] R. Roy and T. Kailath, “ESPRIT-estimation of signal parameters via rotational invariance techniques,” *IEEE Trans. Acoust., Speech, Signal Process.*, vol. 37, no. 7, pp. 984-995, Jul. 1989.
 - [42] M. Braun, “OFDM radar algorithms in mobile communication networks,” Ph.D. dissertation, Dept. Inst. Commun. Eng., Karlsruher Instituts für Technologie, Karlsruhe, Germany, 2014.
 - [43] 3GPP, “3GPP TS 38.104 V17.8.0 (2022-12) 3rd Generation Partnership Project; Technical Specification Group Radio Access Network; NR; Base Station (BS) radio transmission and reception (Release 17),” 2022.
 - [44] 3GPP, “3GPP TS 38.211 V17.4.0 (2022-12) 3rd Generation Partnership Project; Technical Specification Group Radio Access Network; NR; Physical channels and modulation (Release 17),” 2022.
 - [45] T. Haustein, C. von Helmolt, E. Jorswieck, V. Jungnickel, and V. Pohl, “Performance of MIMO systems with channel inversion,” in *Proc. IEEE 55th Veh. Technol. Conf. (VTC Spring)*, vol. 1, May 2002, pp. 35-39.